Original Article

Long-term measurements of fish backscatter from Saildrone unmanned surface vehicles and comparison with observations from a noise-reduced research vessel

Alex De Robertis [1]*, Noah Lawrence-Slavas[2], Richard Jenkins[3], Ivar Wangen[4],
Calvin W. Mordy[2,5], Christian Meinig[2], Mike Levine[1], Dave Peacock[3], and Heather Tabisola[2,5]

[1]*Alaska Fisheries Science Center, National Oceanic and Atmospheric Administration, 7600 Sand Point Way NE, Seattle, WA 98115, USA*
[2]*Pacific Marine Environmental Laboratory, National Oceanic and Atmospheric Administration, 7600 Sand Point Way NE, Seattle, WA 98115, USA*
[3]*Saildrone Inc. Alameda, 1050 W Tower Ave, Alameda, CA 94501, USA*
[4]*Kongsberg Maritime AS, Strandpromenaden 50, P.O. Box 111, 3191 Horten, Norway*
[5]*Joint Institute for the Study of the Atmosphere and Ocean, University of Washington, 3737 Brooklyn Ave NE, Seattle, WA 98195, USA*

Corresponding author: tel: +1-206-526-4789; e-mail: alex.derobertis@noaa.gov.

Two Saildrone unmanned surface vehicles (USVs) were instrumented with echosounders and deployed in the Bering Sea to make acoustic observations of walleye pollock for 103 days. The Saildrones proved to be a suitable platform for measurement of fish backscatter: they produced high-quality measurements at wind speeds of <10 m s^{-1}. Pollock backscatter measured from the Saildrones was compared to backscatter measured by a noise-reduced research vessel during two "follow-the-leader" comparisons. In a location where pollock were shallowly distributed (30–100 m), there was evidence of depth-dependent avoidance reactions to the ship. This behaviour was not evident in a second comparison, where the fish were primarily deeper than 90 m. Opportunistic comparisons indicate that backscatter where the ship and USVs crossed paths was similar. However, the Saildrones observed higher densities of shallow fish, which is consistent with the diving response inferred in the first follow-the-leader comparison. USVs equipped with echosounders, like all platforms, have inherent strengths (endurance) and limitations (species identification) that should be carefully considered for a given application. USVs can complement traditional ship-based surveys by increasing the spatial and temporal extent of acoustic observations, and their use is likely to become more widespread.

Keywords: acoustic survey, autonomous vehicle, unmanned surface vehicle, vessel avoidance

Introduction

Acoustic measurements of fish abundance have been traditionally made from research vessels. Given the high cost of research vessels (National Research Council, 2009), there has been substantial interest in measurement of acoustic backscatter from other platforms such as fishing vessels (Karp, 2007), moorings (Trevorrow, 2005; Brierley *et al.*, 2006), drifters (Lopez *et al.*, 2017), and autonomous underwater vehicles (Brierley *et al.*, 2002). In recent years, compact and highly capable echosounders with low power requirements have become available (Lemon *et al.*, 2012; Benoit-Bird *et al.*, 2018), and there have been substantial advances in autonomous vehicles (Rudnick *et al.*, 2018; Verfuss *et al.*, 2019). Together, these developments have the potential to make long-term acoustic measurements of fish abundance more accessible. Short-duration (<7 day) pilot studies with autonomous surface vehicles (Greene *et al.*, 2014; Swart *et al.*, 2016), ocean gliders

(Guihen *et al.*, 2014), and autonomous underwater vehicles (Moline *et al.*, 2015; Benoit-Bird *et al.*, 2018) equipped with echosounders have produced promising results.

Autonomous vehicles equipped with echosounders have the potential to complement traditional ship-based surveys by increasing the spatial and temporal extent of acoustic observations. Like all platforms used to collect acoustic data, they have inherent strengths and limitations. One attractive capability of some unmanned surface vehicles (USVs) is the potential for long-term (>6 month) deployments (Verfuss *et al.*, 2019). Many of these vehicles use wind or wave power for propulsion and can generate electrical power from solar or wind generators to support the long-term power demand of instrumentation (Meinig *et al.*, 2015; Meyer-Gutbrod *et al.*, 2015). These vehicles are able operate independently of ships in remote study areas, and can transmit data summaries and be controlled remotely via satellite communications. Such USVs may allow for cost-effective long-term acoustic measurements that would not otherwise be possible (Rynne and von Ellenrieder, 2009).

However, the utility of additional acoustic measurements from autonomous vehicles depends largely on overcoming the uncertainties associated with identifying acoustic scatters. Ship-based acoustic–trawl surveys rely on both trawl sampling and acoustic measurements to estimate abundance as a function of species and size (Simmonds and MacLennan, 2005). Thus, barring major developments in species and size identification by acoustic means, USVs are unlikely to replace ship-based surveys used to estimate abundance at age indices used for stock assessment as trawling is not possible. High-latitude areas are favourable environments for echosounder measurements from autonomous vehicles as backscatter can be dominated by a single species. When these conditions are met, long-term deployments of instrumented USVs may allow for a broad range of applications including acoustic indices of abundance (Honkalehto *et al.*, 2011), studies of seasonal changes in abundance/migration patterns (Geoffroy *et al.*, 2011), vessel avoidance (Fernandes *et al.*, 2000), and studies of predator–prey relationships of satellite-tagged top predators (Mordy *et al.*, 2017).

The performance of acoustic instruments is platform-specific and must be evaluated for specific weather conditions. Acoustic instruments installed on surface vehicles may be susceptible to biases introduced by transducer motion (Dunford, 2005) and vehicle orientation (Guihen *et al.*, 2014), as well as attenuation of the transmitted signal by entrained bubbles (Novarini and Bruno, 1982). In addition, acoustic measurements of fish may be affected by avoidance reactions to survey platforms, which can be an important source of error (De Robertis and Handegard, 2013). Fish are presumably more likely to react to large ships than small, quiet USVs.

Here, we describe the integration of a recently developed split-beam autonomous echosounder (Benoit-Bird *et al.*, 2018; De Robertis *et al.*, 2018), with the Saildrone USV (Meinig *et al.*, 2015). We evaluate the potential of Saildrones as a platform for autonomous measurements of fish backscatter during a long-term deployment in the eastern Bering Sea, a low-diversity environment where acoustic scattering is dominated by walleye pollock (Honkalehto *et al.*, 2011). We evaluate the quality of the Saildrone measurements and compare observations of acoustic backscatter made with the Saildrones to those made with a noise-reduced research vessel designed to make high-quality backscatter measurements and minimize avoidance reactions (Mitson, 1995).

Methods

Saildrone USV

The Saildrone generation 3 USV (SD) used in this study is a 5.8 m wind and solar powered autonomous vehicle constructed from carbon fibre (Figure 1a). The vehicle is described by Meinig *et al.* (2015), and is thus only briefly described here. Power for propulsion is supplied by a 4 m wing sail controlled by an actuator reminiscent of an airplane wing flap. The vehicle has three moving parts: small actuators on the tail flap and the rudder, and a rolling-element bearing which allows the vertical wing to rotate. Solar panels on the hull and wing replenish electrical power for vehicle control, communications, and scientific payloads (Meinig *et al.*, 2015). The vehicle navigates autonomously between waypoints provided by the operator. The vehicle communicates to shore via a satellite link every 10 min, allowing for near real-time transmission of data, control of instrumentation, and issuing of waypoints.

Echosounder installation

A fisheries echosounder was added to the SD's suite of meteorological and oceanographic instruments in 2016 (Meinig *et al.*, 2015; Mordy *et al.*, 2017). Simrad split-beam wideband autonomous transceiver (WBAT) split-beam echosounders were integrated with two SD vehicles (SD 126 and SD 128). The WBAT, an existing instrument designed as a self-contained device for use on moorings (De Robertis *et al.*, 2018) was used to evaluate the potential of the SD as a platform for acoustic measurements. The instrument was modified to accept power from SD, and the firmware was altered to allow the instrument to be controlled via serial commands delivered via satellite link. To allow for control of power consumption, 12 min ping ensembles were transmitted at user selectable 12.5–100% duty cycles. The echosounder transmitted 70 kHz narrowband pings every 1.5 s. A 1 ms pulse duration was used to reduce data volumes so that long-term deployments could be conducted with the available storage (data volumes are inversely proportional to pulse duration). The WBAT's timestamp was synchronized with SD's at the beginning of each ensemble. Backscatter data were recorded to a range of 200 m and stored to flash memory inside the WBAT.

An 18° beamwidth 70 kHz Simrad transducer (model ES70-18CD) was mounted on each SD's keel at a depth of 1.9 m (Figure 1a). Like all sail-powered vessels, the SD heels as it moves at an angle to the wind (i.e. there is a consistent roll bias on many points of sail). Although the vehicle also pitches, average pitch is close to zero over long periods, and pitch is lower and less extreme than roll (in deployment described below, pitch averaged 47% of roll). To keep the transducer pointed down as the SD tacked back and forth, the transducer was mounted on a one-way gravity gimbal mount consisting of a hinge allowing ±32° of rotation and a 27 kg lead mass (Figure 1b and c). This mechanism dampened the heeling motion of the transducer, keeping the transducer pointing down and minimizing its motion (Figure 1d). A bend-stable transducer cable (Igus chainflex) and a mechanical bend radius limiter (Figure 1b and c) were employed to minimize cable fatigue as the transducer moved relative to the vehicle.

A series of diagnostic messages reported by the echosounder (e.g. error messages, disk write times, and the number of pings transmitted), were integrated into the SD's data telemetry stream. During the 2016 deployment, the WBAT on one vehicle
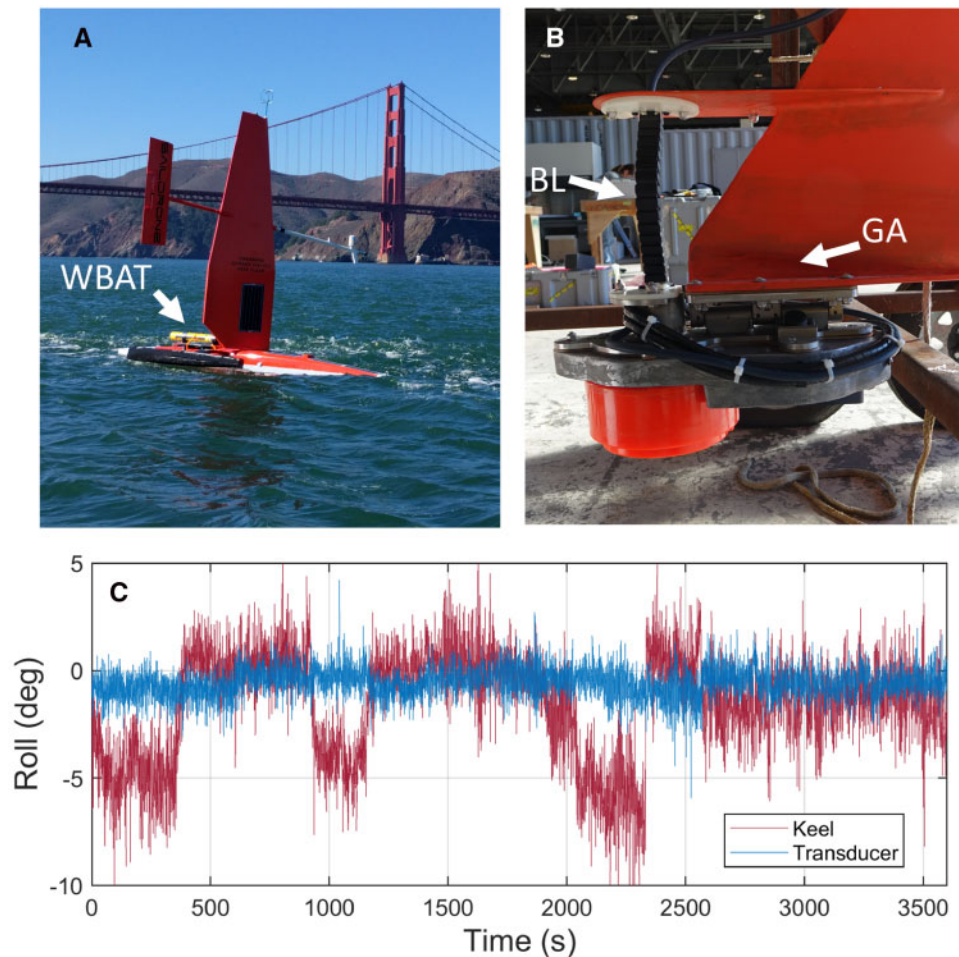
Figure 1. Saildrone vehicle and transducer installation. (a) Saildrone vehicle during initial testing. The WBAT echosounder is mounted on the front of the Saildrone. The instrument was later installed inside the Saildrone. (b) Transducer installed on the keel. Arrows indicate the bend limiter (BL) and gimbal assembly (GA). (c) Roll measured above and below the gimbal showing that the transducer roll is dampened by the gimbal.

experienced a data storage failure, which was identified via an error message. This SD transited to a nearby island (see below for details), where the WBAT was replaced with a prototype WBT Mini echosounder, a more compact but equivalent instrument designed for use on autonomous vehicles (Benoit-Bird *et al.*, 2018).

Echosounder calibration

The WBATs were calibrated using the on-axis standard sphere method (Demer *et al.*, 2015) before and after deployment at a range of 17–25 m with a 38.1 mm tungsten carbide sphere. The before-deployment calibrations were conducted on 28 April 2016 *in situ* with a sphere deployed below the drifting Saildrones. A post-deployment calibration was conducted on 17 November from a boat using the transducer, echosounder, and cabling used on each SD. The WBT Mini was calibrated at the end of the deployment. The gain from the two WBAT calibrations differed by 0.1 dB in the case of SD 126 and 0.3 dB in the case of SD 128. The mean gain (averaged in linear units) was used to process the WBAT data. These repeat calibrations provide an indication of calibration precision: If we had chosen to apply either of the

individual calibrations instead of the mean value, the observed backscatter would differ by 2 or 6%, respectively.

Bering Sea Saildrone deployment

Two Saildrones were deployed from a dock in Dutch Harbor, Alaska on 23 May 2016. They were recovered at the same location 103 days later on 3 September. Together, the Saildrones measured acoustic backscatter over 10 999 km of the southeastern Bering shelf (Figure 2) as part of a multidisciplinary study examining ocean conditions, fishes, and marine mammals (Mordy *et al.*, 2017). A WBAT echosounder on one of the Saildrones failed on 2 July, and the Saildrone navigated to St. Paul Island (Figure 2, 57.1°N 170.3°W), where the WBAT was replaced with the WBT Mini prototype on 14 July. The echosounders were operated at a 100% duty cycle until 14 August after which they were operated at 50 or 25% duty to reduce power consumption as shorter days began to limit the power generated by the solar panels.

Acoustic–trawl survey

The NOAA ship *Oscar Dyson* (DY), a 64-m noise-reduced research vessel conducted an acoustic–trawl survey of walleye pollock (*Gadus chalcogrammus*) concurrently (12 June–17 August)
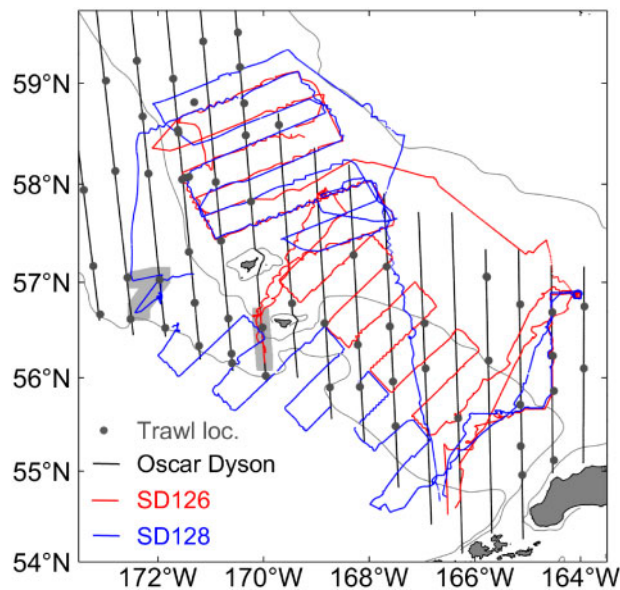
Figure 2. Map showing where Saildrone acoustic data were collected, the locations of *Oscar Dyson* survey transects, and trawl sites ($n = 62$). The locations of follow-the-leader comparisons are indicated by the thick grey shading. The 50, 100, and 200 m depth contours are depicted by grey lines.

with the Saildrone deployment. During this survey (Figure 2), acoustic backscatter was measured during daylight hours on transects spaced 37 km apart, and targeted trawls were used to identify acoustic scatterers (Honkalehto and McCarthy, 2015). Observations from DY's 70 kHz Simrad EK60 echosounder were compared to measurements from SD. A 7° beamwidth ES70-7C transducer was operated at a 1 s ping rate and 0.5-ms pulse length, which is a narrower beam and a shorter pulse than used by SD. The echosounder was calibrated on 13 June and 16 August 2016 in the same fashion as SD's instruments. The mean estimate of gain from both calibrations was applied in processing: gain from these calibrations differed by 0.1 dB. Trawl sampling confirmed that as in previous years (Honkalehto *et al.*, 2011; Honkalehto and McCarthy, 2015) semi-demersal fishes in the study area were dominated by walleye pollock. In 61 pelagic and bottom trawls targeting acoustically detected fish aggregations in the study area (Figure 1), pollock comprised 92.7% of catch weight. The second-most common species in these catches was *Chrysaora melanaster*, a weakly scattering jellyfish (De Robertis and Taylor, 2014) which accounted for 4.7% of catch weight. Thus, acoustic backscatter in the study area was primarily attributable to pollock.

Follow-the-leader comparison

DY interrupted the survey and conducted two "follow-the-leader" comparisons, one with each SD. A location where spatially extensive aggregations of pollock were observed was identified (Figure 2). SD navigated in a straight line with the echosounder operating at a 100% duty cycle. DY matched course and speed, trailing SD by 500 m. DY was offset by 100 m to starboard to facilitate navigation. SD and DY made a single turn during each comparison. A trawl was deployed at each site to confirm the size and species composition of the fishes.

The first comparison (SD 126) was conducted from 0025 to 2158 on 10 July in water depths of 95–121 m and winds averaging 5.5 m s^{-1} (range: 1.4–11.5 m s^{-1}). Pollock accounted for 99.7% of the trawl catch by weight, and fork length averaged 41 cm (90% were 38–45 cm). The vehicles travelled 73 km at average speed of 1.0 m s^{-1} (range: 0.1–1.8 m s^{-1}). The second comparison (SD 128) was conducted from 1805 to 1300 on 19–20 July, in water depths of 114–132 m and winds averaging 8.7 m s^{-1} (range: 5–13.3 m s^{-1}). Pollock accounted for 99.8% of the catch, and length averaged 45 cm (90% were 40–51 cm). The vehicles travelled 89 km at a mean speed of 1.4 m s^{-1} (range: 0.9–2.1 m s^{-1}).

The measurements from DY and SD were aligned into elementary distance sampling units (EDSUs) of 2 km by finding the along-track segments for SD closest to each 2 km section of DY's trackline. Data while the vehicles were turning were excluded. This resulted in 33 EDSU's for the first comparison and 42 for the second.

Large-scale comparison

To complement the follow-the-leader comparisons, we compared backscatter measurements when SD and DY crossed paths during the larger-scale survey. Given the use of equivalent vehicles and instrumentation, the SDs were assumed to produce equivalent results and observations from both SDs were pooled. Areas where SD and DY crossed paths within 20 km and 7 days of each other were identified (Supplementary Figure S1, $n = 17$ locations, 365 DY EDSUs and 571 SD EDSUs). Bottom depth at the comparison sites ranged from 70 to 118 m. Only daytime SD observations were used to match the daytime DY survey.

Data processing

Echosounder measurements from SD and DY were processed with Myriax Echoview 8.0.86. In the case of the follow-the-leader comparisons, data from 12 m below the sea surface to 0.5 m above the sounder-detected bottom (determined with Echoview's best bottom candidate algorithm) were integrated using a −70 dB re 1 m^{-1} integration threshold in 100-m along-track and 1-m vertical bins. The large-scale comparison was processed over a slightly different scale to match the available archived DY survey data: data from 16 m depth to 1 m above bottom were exported in 1000-m along-track and 1-m deep bins.

The data sets differ in that the SDs exhibited evidence of attenuation of the acoustic signal from surface bubbles swept below the transducer at wind speeds >10 m s^{-1} (i.e. there was evidence of backscatter from surface bubbles, and/or signs that the transmitted signal was attenuated by bubbles as sea state increased). In contrast, DY is equipped a centreboard extending to 9.15 m, and the echosounder is thus much less sensitive to bubble attenuation (Shabangu *et al.*, 2014). As a first-order correction we identified and excluded SD pings with a locally weak bottom echo or a perturbed index of the transmit pulse as these indicate attenuation of the echosounder signal (Honkalehto *et al.*, 2011; Ryan *et al.*, 2015). Pings where the maximum bottom echo was 6 dB lower than that computed over a 61 ping running median were excluded. In addition, pings where an index of the transmit pulse (mean S_v from 0 to 3 m range) differed by >0.1 dB (2.3% in linear terms) from the median value in a 61 ping running window were excluded (Honkalehto *et al.*, 2011). In areas where the bottom echo was not recorded (i.e. depths >195 m), only the transmit pulse criterion was applied.

Because the echosounder used on SD had a wider beamwidth and longer pulse length, the near-bottom acoustic dead zone (ADZ) where fish cannot be detected near the seafloor is larger for SD. At 100 m range, the ADZ is 2.6 m for SD and 0.8 m for DY (Ona and Mitson, 1996). We thus implemented a correction (Ona and Mitson, 1996) to compensate for this effect. Backscatter above the sounder-detected bottom (0.5–2 m above bottom for the follow-the-leader and 1–2.5 m for the large-scale comparison) was integrated and extrapolated into the ADZ. This correction assumes a flat bottom over the beam footprint, which is reasonable for the low-relief eastern Bering Sea. This correction was modest: mean water column backscatter observed by SD/DY increased by 2.3/1.0% in the first follow-the-leader comparison and 1.8/1.3% in the second.

Statistical analysis

We applied methods used in previous vessel comparisons (Kieser *et al.*, 1987) to estimate the vessel backscatter ratio (i.e. $R = (s_{A,SD} + ADZ_{SD})/s_{A,DY} + ADZ_{DY})$ where s_A is the nautical area scattering coefficient (MacLennan *et al.*, 2002), and ADZ is the dead zone correction. R can be derived from the mean difference in log-transformed backscatter observations in the paired EDSU's

$$R = \exp\left(n^{-1} \sum_i^n \left(\ln(s_{A,SD,i} + ADZ_{SD,i}) - \ln(s_{A,DY,i} + ADZ_{DY,i}) \right) \right),$$

where i denotes the EDSU, and n the total number of EDSUs. The differences between the two platforms [i.e. $\ln(s_{A,SD} + ADZ_{SD}) - \ln(s_{A,DY} + ADZ_{DY})$] were not significantly autocorrelated ($p > 0.05$) at the 2 km EDSU distance. The backscatter differences can be expressed in terms of a per cent difference relative to the DY observations [i.e. $(R-1)\cdot 100$].

The vertical distribution of backscatter was summarized as the mean weighted depth for each EDSU

$$mwd_i = \frac{\sum_l (d_l \cdot s_{A,l,i})}{\sum_l s_{A,l,i}},$$

where d is the depth (m) of layer l.

The difference in mwd between SD and DY was computed as

$$D = n^{-1} \sum_i^n (mwd_{SD,i} - mwd_{DY,i}).$$

As the transducer depths are different for SD and DY, only the commonly observed depths (>12 m for the follow-the-leader comparisons, and >16 m for the large-scale comparisons) were compared. Note that mwd will be slightly deeper for DY than SD in cases where fish are close to the seafloor as DY's echosounder can resolve targets closer to the seafloor.

Approximate bootstrap confidence intervals for R and D were estimated by drawing bootstrap samples with replacement from the EDSUs. In each bootstrap realization, a series of n EDSUs was drawn at random from the original observations with replacement. Approximate 95% confidence intervals were estimated by finding the 2.5 and 97.5% percentiles of R and D from 5000 bootstrap realizations.
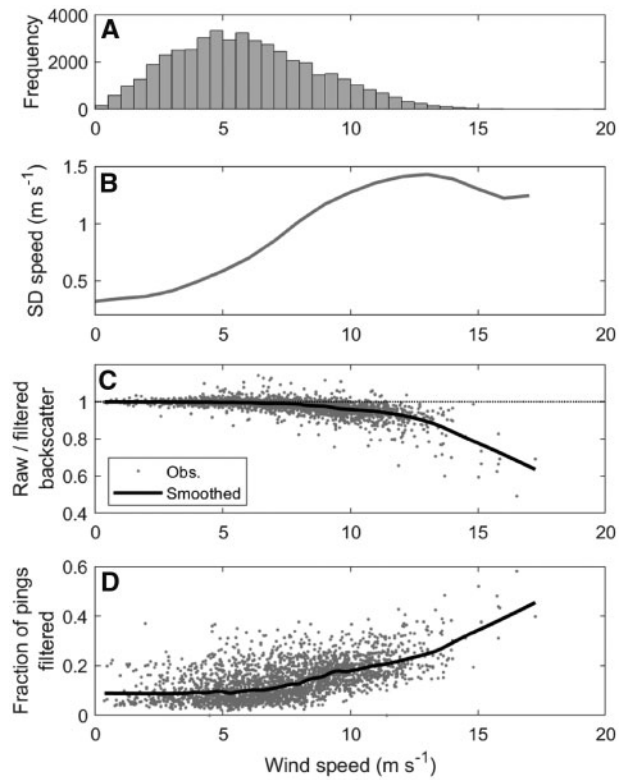

Figure 3. Wind speeds and relationship with Saildrone speed and backscatter observations. (a) Distribution of 5-min averaged wind speed observations. (b) Mean Saildrone speed as a function of wind speed. (c) Effect of removing pings showing evidence of bubble attenuation as a function of wind speed expressed as the ratio of backscatter computed with all pings and only those passing the filter criteria. (d) Fraction of pings removed by the filter. Panels (c) and (d) are derived from analysis of a subset of SD data (4087 1-km EDSUs). The black lines indicate a LOWESS smooth ($f = 0.1$, Cleveland, 1979).

Results

Saildrone speed in relation to wind

Wind speeds were generally low during the deployment, averaging 5.9 ± 2.8 m s^{-1} (5 min averages $\pm$ *SD*) with 95% of wind speeds <11 m s^{-1}, and maximum wind speeds of 19.5 m s^{-1} (Figure 3a). The Saildrones travelled at an average speed of 0.7 ± 0.5 m s^{-1}, achieving a maximum speed of 3.9 m s^{-1}. As a wind-powered vehicle, the Saildrones cannot sail upwind, and must tack at angles to the wind to move upwind. Averaged over all points of sail, the Saildrones travelled at ∼12% of the wind speed, moving at 0.6 m s^{-1} at wind speeds of 5 m s^{-1} and 1.3 m s^{-1} at wind speeds of 10 m s^{-1} (Figure 3b). At wind speeds >13 m s^{-1}, SD speed no longer increased with wind speed (Figure 3b), likely due to increased sea states.

Saildrone echosounder measurements

Backscatter measurements from the Saildrones were free from obvious artefacts (Figure 4), except at the highest wind speeds, where near-surface backscatter from bubbles was evident. Comparison of backscatter from all pings and only those passing the criteria used to identify bubble attenuation indicated that, as
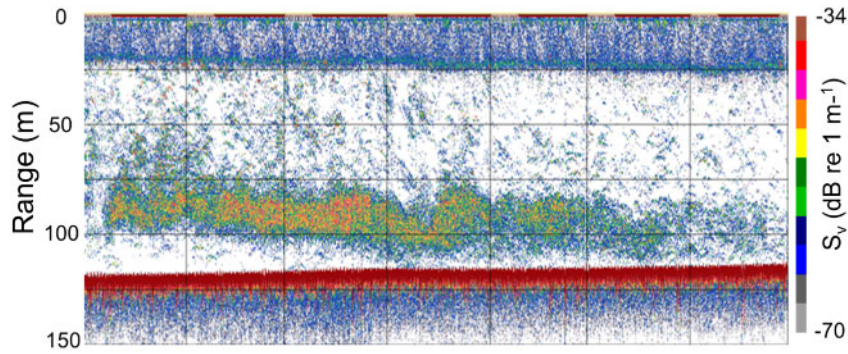
Figure 4. Echogram depicting an aggregation of walleye pollock at depths of 75–125 m. Wind speed was 8 m s^{-1}.
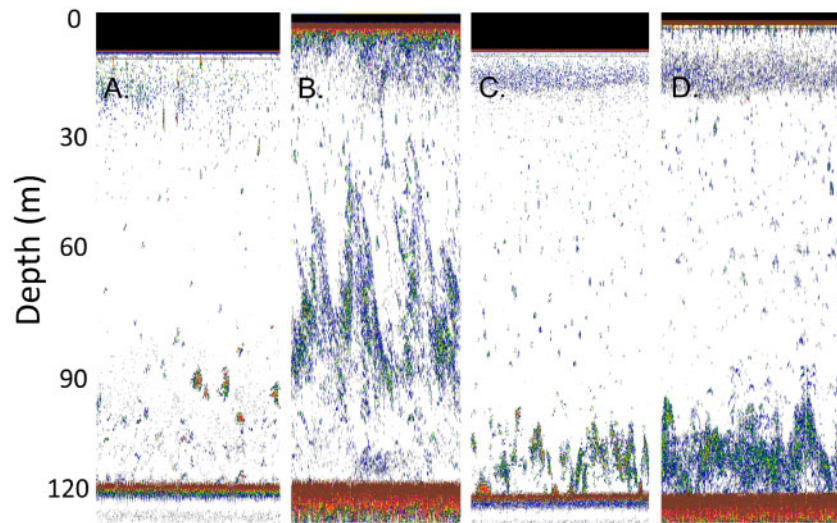

Figure 5. Echograms from the follow-the-leader comparisons. During the first comparison it was evident that (a) DY consistently detected less backscatter from shallow pollock backscatter than (b) SD. During the second comparison, the depth distribution from (c) DY and (d) SD was more similar. Note that SD's wider beam samples a larger volume and fish schools thus appear larger and more diffuse. Colour scale as in Figure 4.

expected, including pings with evidence of bubble attenuation lowered backscatter measurements (Figure 3c). The impact of wind speed on the correction was nonlinear: at wind speeds of 10 m s^{-1}, the raw measurements were ∼4% lower than when the filters were applied, and the discrepancy increased sharply at higher wind speeds. As wind speed increased past 5 ms^{-1}, the fraction of pings removed by these criteria approximately doubled for every 5 m s^{-1} increase in wind speed (Figure 3d).

Follow-the-leader comparisons

The first follow-the-leader comparison exhibited discrepancies in the amount and depth distribution of pollock backscatter, consistent with shallow pollock reacting more to DY than SD. SD consistently detected more backscatter from shallow pollock (Figure 5a and b), particularly at night (Figure 6a and c). Water column backscatter from SD was 15% higher than from DY ($R = 1.15$ [1.02–1.28], $-X$ [95% CI]). SD observed shallower distributions during the day, and greater backscatter at night. During daytime, both platforms recorded similar backscatter (Figure 6a and b, $R = 1.04$ [0.87–1.24]). However, backscatter observed by SD was consistently shallower than that observed by DY

(Figure 6a, $D = -4.6$ m, [-8.7 to -0.4 m]). At night, SD observed 29% greater backscatter (Figure 6a and b, $R = 1.29$, [1.17–1.43]) than DY. This was primarily due to SD's observations of greater backscatter between 30 and 60 m (Figure 6c). Observations at approximately >70 m were similar (Figure 6c). SD detected shallower backscatter than DY at night (Figure 6b), but this was not significantly different (D of -6.5 m [-14.5 to 2.0 m]).

In contrast, in the second comparison, there were no obvious differences when comparing the echograms or backscatter time series (Figures 5 and 7). Pollock were patchier and distributed deeper and closer to the bottom than in the first comparison (Figures 5 and 7b and c). On average, SD observed ∼11% less backscatter than DY ($R = 0.89$, [0.81–0.99]). However, this difference is no longer significant if a single compact high-abundance school detected by DY during daytime (Figure 7a) is excluded ($R = 0.91$, [0.83–1.0]). Overall, the depth distribution of backscatter observed from SD and DY was equivalent (Figure 7b and c, $D = 1.2$ m, [-0.2 to 2.7 m]). During daytime, backscatter from SD was ∼14% less than from DY ($R = 0.86$, [0.76–0.97]). Mean-weighted depth from DY was slightly deeper
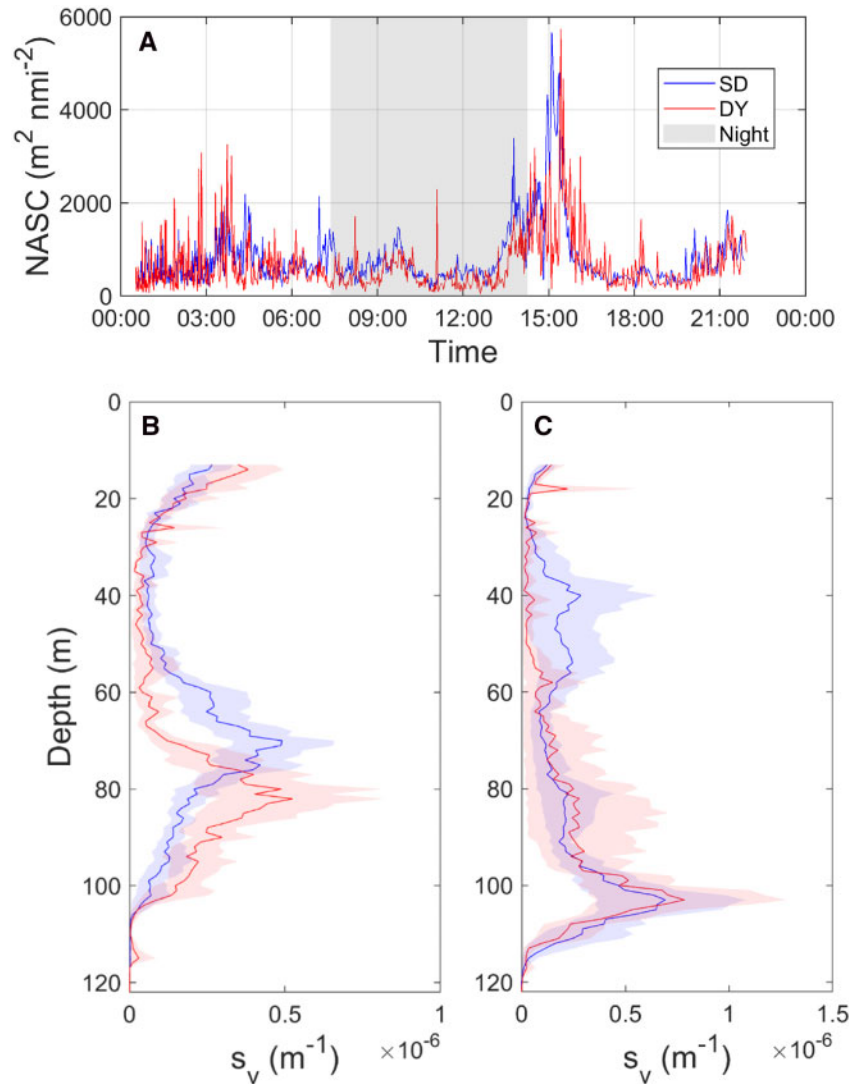
Figure 6. First follow-the-leader comparison. (a) Backscatter time series with night indicated by grey shading. Average backscatter during the comparison period shown in 1 m bins during (b) day and (c) night. The bands show bootstrapped 95% confidence intervals.

($D = -2.6$ m, [-4.7 to -0.5 m]). However, the difference in depth distribution is sensitive to the method used summarize the vertical distribution. Although *mwd* was deeper from DY, backscatter from DY was shallower when the vertical distribution is computed as the average over the entire comparison (Figure 7b). This discrepancy is because this calculation weights high-abundance locations more heavily than the *mwd* analysis. Furthermore, the difference in *mwd* was no longer significant when the ADZ correction was added to the deepest depth bin in the EDSU prior to calculating *mwd* ($D = -1.8$ m, [$CI -4.0$ to 0.1 m]). Together this suggests that the interpretation of depth difference in the second comparison is questionable as the conclusions are sensitive to the analysis method. At night, the backscatter ($R = 0.97$, [$0.81–1.15$]) and depth distribution ($D = -0.3$ m, [-3.1 to 3.1 m]) from SD and DY were equivalent.

We considered two potential explanations for the lower daytime backscatter observed by SD in the second comparison. One possibility is that there was elevated attenuation of SD's echosounder transmissions by near-surface bubbles due to a shallower transducer. However, winds were similar during day and night, averaging 8.5 m s^{-1} (range: 5.2–11.6) during daytime, and 8.6 m s^{-1} (range: 7.5–9.5) at night. Furthermore, the vessel ratio R observed in a given EDSU was not correlated with wind speed ($r = 0.001$, $p < 0.05$). Finally, daytime near-surface backscatter which would also be affected by this mechanism was similar for SD and DY, (Figure 7b, R for upper 30 m was 0.96 [0.89–1.03]). Thus, attenuation by near-surface bubbles is unlikely to explain the observed discrepancy.

Another possibility is that the near-bottom pollock present during the daytime during the second comparison were less likely to be observed by SD, which has a larger near-bottom ADZ. The ADZ correction assumes that fish density above the unobserved near-bottom zone is equivalent to that in the adjacent observed zone (Ona and Mitson, 1996). The correction will be an underestimate if fish abundance increases substantially in close proximity to the bottom as in these observations (Figure 7). The vessel ratio close to the seafloor where the ADZ effect will be highest (from 1 to 5 m above the seafloor echo) shows that SD detected
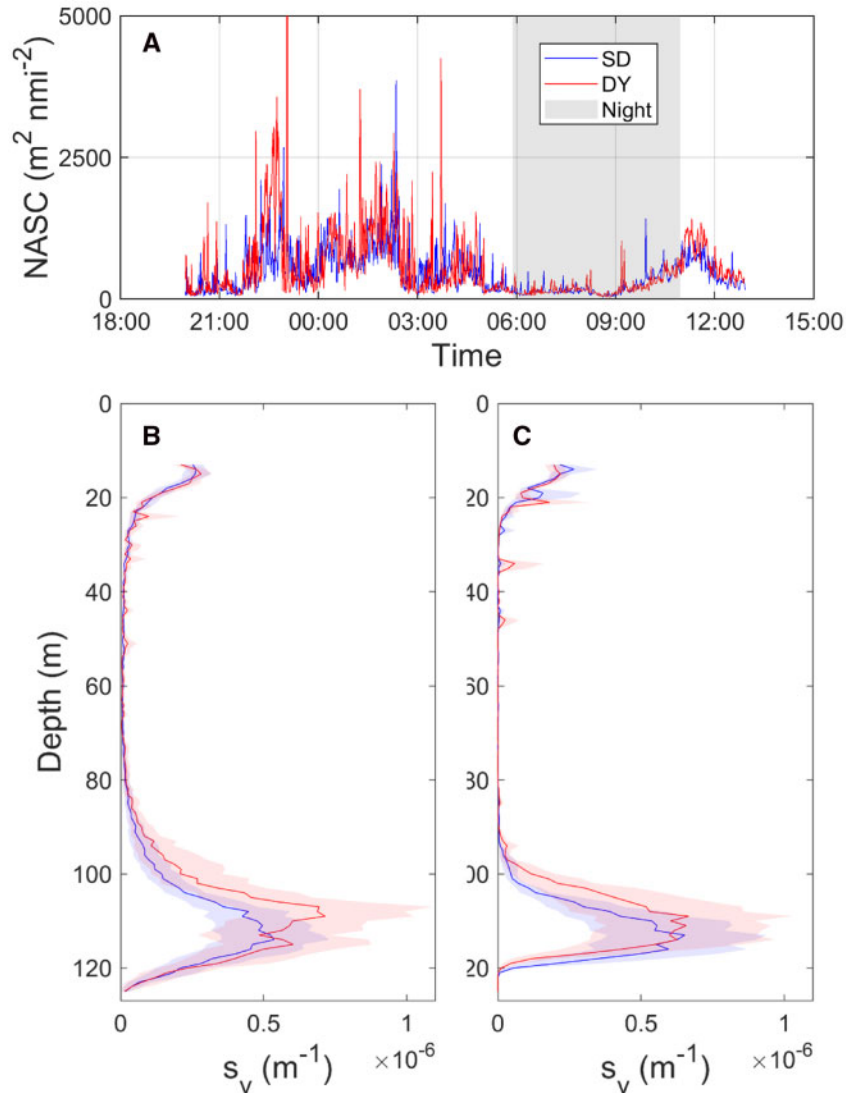
Figure 7. Second follow-the-leader comparison. (a) Backscatter time series with night indicated by grey shading. Note that scale is truncated to exclude a single high-backscatter aggregation (11 000 m^2 nmi^{-2}) observed by DY at 2304. Average backscatter during the comparison period shown in 1 m bins during (b) day and (c) night. The bands show bootstrapped 95% confidence intervals.

substantially less backscatter than DY even after ADZ correction (R = 0.76, [0.59–0.97]). In contrast, >5 m above bottom the observations from SD and DY were not significantly different (R = 0.91, [0.78–1.04]). This indicates that the observed differences are at least partially attributable to differences in the ability of SD and DY to detect fish near the seafloor.

Large-scale comparison

Overall, average backscatter from SD and DY was similar but the depth distributions differed (Figure 8a and b). Over the water column, SD detected equivalent backscatter to DY (Figure 8b, R = 1.09, [0.93–1.27]). SD observed greater backscatter than DY at <70 m, while DY measured higher backscatter at >100 m (Figure 8a). At <30 m, where backscatter was dominated by a near-surface layer of unknown origin (Figures 4 and 5) DY and SD measured similar backscatter (Figure 8b). However, at depths >30 m where backscatter in this survey is dominated by walleye

pollock SD tended to detect higher abundances of pollock in shallow water (Figure 8a). For example, at depths of 30–70 m SD observed 40% greater backscatter than DY (R = 1.40, [1.06–1.92]). However, at >70 m DY tended to record higher values (Figure 8a) but this was not significantly different (Figure 8b). SD detected consistently shallower backscatter than DY. On average, backscatter was 4.9 m shallower from SD than DY (Figure 8c, D = −4.9 m [−8.7 to −1.2 m]). This was driven by the depth distribution of pollock at >70 m, which were consistently deeper when detected by DY than SD (Figure 8c). These results are not sensitive to the time window used in the comparison (Supplementary Figure S2).

Discussion

Backscatter measurement from Saildrones

Ocean-going robotic vehicles and low-power echosounders suitable for use with these vehicles have advanced substantially in
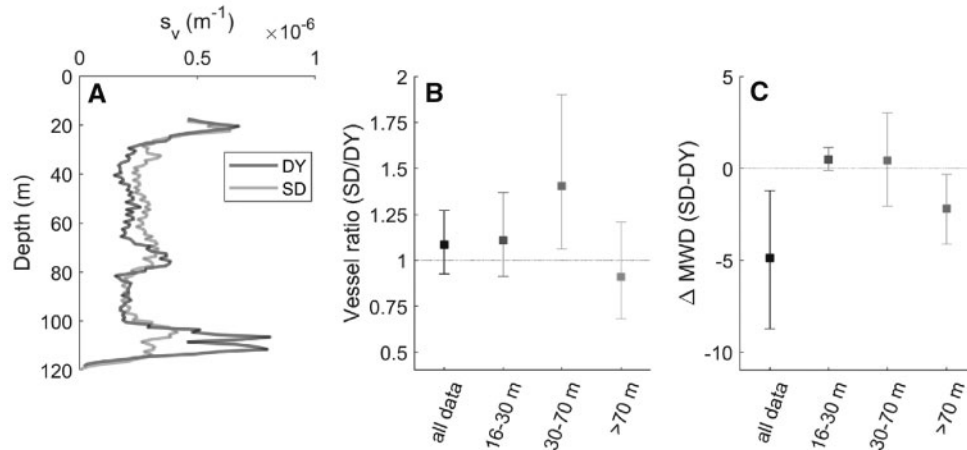
Figure 8. Summary of large-scale comparison. (a) Average backscatter in 1-m depth bins. (b) Vessel ratio calculated for several depth zones. (c) Difference in backscatter mean weighted depth calculated for several depth zones.

recent years (Verfuss *et al.*, 2019). Although USVs have been instrumented with fisheries echosounders in the past, deployments have generally been limited to short-duration demonstration studies (Greene *et al.*, 2014; Swart *et al.*, 2016). This study demonstrates that it is now practical to make routine long-term measurements of acoustic backscatter over a wide area with an USV equipped with an echosounder equivalent to those used in fisheries surveys. The echosounder used in this study (Benoit-Bird *et al.*, 2018; De Robertis *et al.*, 2018) is capable of split-beam operation, which allows for accurate calibration and estimation of fish target strength (Ona, 1999) as well as multi-frequency and broadband operation, which allows scatterers to be better characterized (Bassett *et al.*, 2017; Korneliussen, 2018). Solar charging allowed for operation of the echosounder and an extensive suite of meteorological and oceanographic instruments (Mordy *et al.*, 2017) during a deployment exceeding 100 days. The SDs exhibited considerable operational flexibility. Ships were not required for deployment or recovery: the vehicles were deployed from a dock and transited to a remote study area. A vehicle transited to an accessible location to address an instrument malfunction.

Overall the Saildrones produced echo-integration measurements of good quality, but there was evidence for degradation of the measurements at higher wind speeds (>10 m s^{-1}) due to bubbles entrained under the transducer (Novarini and Bruno, 1982). These wind speeds are similar to those at which bubble attenuation becomes a concern with hull-mounted echosounders on ships (Shabangu *et al.*, 2014; Delacroix *et al.*, 2016) and USVs (Swart *et al.*, 2016). Acoustic measurements from near-surface transducers (regardless of platform) are subject to degradation by bubbles at higher sea states, which will limit the conditions under which high-quality data can be collected. If adverse conditions occur a small fraction of the time, this can be mitigated by pausing surveys at higher sea states.

Autonomous vehicles and low-power instruments suitable for these vehicles are currently undergoing a period of rapid development (Rudnick *et al.*, 2018; Verfuss *et al.*, 2019). There have been several developments in the Saildrone vehicles since this study. In subsequent work we have used the more compact WBT Mini echosounder (Benoit-Bird *et al.*, 2018), and a dual-frequency (38 kHz split-beam, 200 kHz single beam) transducer. This transducer was selected as 38 kHz is the frequency most used in

acoustic–trawl surveys of fish (Simmonds and MacLennan, 2005), and it is less sensitive to bubbles (Novarini and Bruno, 1982; Delacroix *et al.*, 2016). Multiple frequencies and broadband operation will allow for additional characterization of the acoustic targets (Bassett *et al.*, 2017). We have added the capability to summarize echosounder data and transmit them to shore (Supplementary Figure S3), which allows the vehicle to be adaptively tasked in response to the echosounder observations (Moline *et al.*, 2015; Swart *et al.*, 2016). The current 5th generation Saildrone is larger, can provide more power, and is substantially faster (Supplementary Figure S4).

Comparison of backscatter observed from Saildrones and a research vessel and evidence of avoidance reactions

The echosounder measurements from the Saildrones compared well to those from the *Oscar Dyson*, a state-of-the-art research vessel. However, there were consistent differences during the first follow-the-leader comparison, with the Saildrones recording consistently more or shallower fish backscatter than the research vessel. If pollock did not react to DY, one would expect both SD and DY to observe equivalent backscatter and depth distributions. The observed differences are attributed to vessel avoidance reactions to DY, which is a noise-reduced vessel designed to minimize avoidance reactions (Mitson, 1995; De Robertis and Handegard, 2013). SD, which was 500 m in front of DY, is likely to have observed the undisturbed behaviour of pollock (pollock have been observed to react to ships at ranges of 270 m, De Robertis and Wilson, 2010). During daytime, SD observed consistently shallower pollock distributions, but similar total backscatter as DY, which is consistent with a diving response (Ona *et al.*, 2007). In contrast, at night, when pollock were more shallowly distributed, SD observed higher backscatter at <70 m, which is consistent with lateral avoidance and/or changes in fish orientation in response to DY (De Robertis and Handegard, 2013). Although the day/night differences in behaviour are unexplained, they are consistent with previous observations of pollock exhibiting stronger vessel avoidance responses at night (De Robertis and Wilson, 2010; De Robertis and Handegard, 2013).

In contrast, during the second follow-the-leader comparison, DY detected more backscatter than SD (∼11% more overall and ∼14% more during daytime). However, this difference is likely attributable to differences in instrumentation rather than fish avoidance reactions. Pollock were distributed close to the bottom throughout the second comparison. The echosounder used on DY is able to resolve fish closer to the seafloor than the echosounder used on SD due to the use of a narrower-beam transducer and a shorter pulse length. We applied an ADZ correction (Ona and Mitson, 1996), but the correction assumes that fish abundance is uniform with respect to height above the seafloor, and that the echosounder's beam is perpendicular to a flat seafloor. In practice, the correction will be an under-estimate as pollock are likely to be more abundant in the ADZ than the observed area directly above the ADZ (Kotwicki et al., 2013) and the beam may not be completely perpendicular to the seafloor.

Other differences in instrumentation may also play a role. The EK60 instrument slightly overestimates backscatter from low densities of fish at longer ranges by up to ∼20%, (De Robertis et al., 2019), which may contribute to the higher backscatter observations from DY than SD. In addition, calibration uncertainty was not included in the error bounds, and, based on the use of 1–2 calibrations, this adds uncertainty of ∼10 to 20% to the vessel ratio (De Robertis et al., 2019).

The large-scale comparison of daytime echo integration measurements from SD and DY was consistent with the follow-the-leader comparisons. Overall, SD detected equivalent backscatter to DY (to within 10%), which is consistent with the agreement in previous comparisons of acoustic measurements from a USV and a research vessel (Swart et al., 2016), different vessels (De Robertis and Handegard, 2013), and different instruments on the same vessel (Macaulay et al., 2018). However, there were differences in vertical distribution. SD consistently detected pollock to be shallower than DY, which supports the inference that shallow pollock dive in response to DY. This implies that the depth-distribution from these daytime pollock surveys (but not the vertically integrated backscatter) may be biased deep due to vessel avoidance. However, one should keep in mind that the observations in this study were made at 70 rather than 38 kHz, the primary frequency used in survey. Scattering from fishes is more directional at higher frequencies (Foote, 1985), and if fish dive as DY approaches, the expected reduction in backscatter will be smaller at 38 kHz.

These observations along with the follow-the-leader comparisons provide further evidence that noise-reduction of research vessels (Mitson, 1995; Fernandes et al., 2000) does not guarantee the elimination of fish reactions (De Robertis and Handegard, 2013). This is the case even for slow vessel speeds at which vessels such as DY emit substantially less radiated noise than at survey speed (Mitson, 1995). Avoidance reactions are difficult to quantify (Ona et al., 2007; De Robertis and Handegard, 2013), and acoustic measurement of fish with autonomous vehicles may ultimately reveal that vessel avoidance reactions are more widespread than was previously recognized.

Applications of echosounder-equipped USVs

Autonomous vehicles are becoming accessible as acoustic survey platforms and have the potential to facilitate studies covering temporal and spatial scales that would not otherwise be possible (Powell and Ohman, 2015; Verfuss et al., 2019). However, one must recognize the limitations of the approach. For example, many fisheries agencies conduct ship-based acoustic–trawl surveys to inform fisheries management. Given that requirements for ships and staff to make measurements at sea may outstrip available resources, there is interest in using autonomous vehicles as a substitute for ships in these surveys (Greene et al., 2014). However, these surveys rely on temporally concurrent acoustic and trawl measurements to estimate abundance as a function of species/size/age. Trawl measurements are a critical component of these surveys and they cannot be made from autonomous vehicles. It will prove difficult for wind or wave-powered USVs to remain in close proximity with a trawl-capable ship conducting a survey as USV speeds are slow and unpredictable relative to the ship, leading to substantial time lags between USV acoustic observations and the ship-based trawls. Although there is potential in some cases to infer the species and size composition of sound scatterers from acoustic measurements alone (Stanton et al., 2010; Bassett et al., 2017; Korneliussen, 2018) these methods, in their current state, are not a sufficient replacement for trawl sampling in most applications. Until it can be convincingly demonstrated that this key limitation can be overcome, autonomous vehicles should be considered a way to augment rather than replace the capabilities of ships in such surveys, for example by using autonomous vehicles on reconnaissance missions to identify areas or time periods where more extensive sampling with research vessels is warranted (Swart et al., 2016).

Autonomous vehicles are thus best used in applications where increased spatial and temporal coverage is beneficial and the lack of concurrent biological sampling is not a critical limitation. In some environments (e.g. low-diversity high latitude ecosystems), it will be possible to ascribe acoustic backscatter to dominant species (Geoffroy et al., 2011; Honkalehto et al., 2011). In other instances, it may be possible to develop robust acoustic-derived measures of key trophic/functional groups to support ecosystem-based management (Trenkel et al., 2011; Ressler et al., 2012; Godø et al., 2014). USVs aslo have the ability to transit to remote study areas and conduct adaptive survey designs in response to real-time observations. For example, USVs can be used to inform the decision of where/when to survey most effectively with ships, and conduct studies of fish migrations, vessel avoidance, and prey availability of satellite-tracked predators. USVs are becoming increasingly accessible, and their use for a wide range of applications is likely to increase in the near future.

There have been rapid advances in autonomous vehicles and acoustic instruments in recent years, and it is clear that high-quality acoustic echo-integration measurements are possible from autonomous platforms (Brierley et al., 2002; Greene et al., 2014; Moline et al., 2015; Swart et al., 2016). This work builds on these studies, extends the duration of these deployments, and provides further support to the idea that echosounder measurements comparable to those from research vessels are possible from USVs over extended temporal and spatial scales. Looking to the future, the key challenge is not how to make backscatter measurements from autonomous surface vehicles, but rather how to best apply the capabilities of autonomous platforms instrumented with echosounders in studies of marine ecosystems. To this end, future work should focus on applied studies evaluating how autonomous platforms can advance understanding of the abundance, distribution, and behaviour of marine organisms.

Acknowledgements

Supplementary data

Supplementary material is available at the *ICESJMS* online version of the manuscript.

Funding

References

Bassett, C., De Robertis, A., and Wilson, C. 2017. Broadband echosounder observations of frequency response during from fisheries surveys in the Gulf of Alaska. ICES Journal of Marine Science, 75: 1131–1142.

Benoit-Bird, K. J., Welch, T. P., Waluk, C. M., Barth, J. A., Wangen, I., McGill, P., Okuda, C. et al. 2018. Equipping an underwater glider with a new echosounder to explore ocean ecosystems. Limnology and Oceanography: Methods, 16: 734–749.

Brierley, A. S., Fernandes, P. G., Brandon, M. A., Armstrong, F., Millard, N. W., McPhail, S., Stevenson, P. et al. 2002. Antarctic krill under sea ice: elevated abundance in a narrow band just south of the ice edge. Science, 295: 1890–1982.

Brierley, A. S., Saunders, R. A., Bone, D. G., Murphy, E. J., Enderlein, P., Conti, S. G., and Demer, D. A. 2006. Use of moored acoustic instruments to measure short-term variability in abundance of Antarctic krill. Limnology and Oceanography: Methods, 4: 18–29.

Cleveland, W. S. 1979. Robust locally weighted regression and smoothing scatterplots. Journal of the American Statistical Association, 74: 829–836.

Delacroix, S., Germain, G., Berger, L., and Billard, J. Y. 2016. Bubble sweep-down occurrence characterization on Research Vessels. Ocean Engineering, 111: 34–42.

Demer, D. A., Berger, L., Bernasconi, M., Bethke, E., Boswell, K., Chu, D., Domokos, R. et al. 2015. Calibration of acoustic instruments. ICES Cooperative Research Reports, 326: 133.

De Robertis, A., Bassett, C., Andersen, L. N., Wangen, I., Furnish, S. R., and Levine, M. 2019. Amplifier linearity accounts for discrepancies in echo-integration measurements from two widely used echosounders. ICES Journal of Marine Science, 76: 1882–1892.

De Robertis, A., and Handegard, N. O. 2013. Fish avoidance of research vessels and the efficacy of noise-reduced vessels: a review. ICES Journal of Marine Science, 70: 34–45.

De Robertis, A., Levine, R., and Wilson, C. 2018. Can a bottom-moored echosounder array provide a survey-comparable index of abundance? Canadian Journal of Fisheries and Aquatic Sciences, 75: 239–640.

De Robertis, A., and Taylor, K. 2014. *In situ* target strength measurements of the scyphomedusa *Chrysaora melanaster*. Fisheries Research, 153: 18–23.

De Robertis, A., and Wilson, C. D. 2010. Silent ships sometimes do encounter more fish. Part II: concurrent echosounder observations from a free-drifting buoy and vessels. ICES Journal of Marine Science, 67: 996–1003.

Dunford, A. J. 2005. Correcting echo-integration data for transducer motion. Journal of the Acoustical Society of America, 118: 2121–2123.

Fernandes, P. G., Brierley, A. S., Simmonds, E. J., Millard, N. W., McPhail, S. D., Armstrong, F., Stevenson, P. et al. 2000. Fish do not avoid survey vessels. Nature, 404: 35–36.

Foote, K. G. 1985. Rather-high-frequency sound scattering by swim-bladdered fish. Journal of the Acoustical Society of America, 78: 688–700.

Geoffroy, M., Robert, D., Darnis, G., and Fortier, L. 2011. The aggregation of polar cod (*Boreogadus saida*) in the deep Atlantic layer of ice-covered Amundsen Gulf (Beaufort Sea) in winter. Polar Biology, 34: 1959–1971.

Godø, Ø. R., Handegard, N. O., Browman, H. I., Macaulay, G. J., Kaartvedt, S., Giske, J., Ona, E. et al. 2014. Marine ecosystem acoustics (MEA): quantifying processes in the sea at the spatio-temporal scales on which they occur. ICES Journal of Marine Science, 71: 2357–2369.

Greene, C. H., Meyer-Gutbrod, E. L., McGarry, L. P., Hufnagle, L. C., Chu, D., McClatchie, S., Packer, A. et al. 2014. A wave glider approach to fisheries acoustics transforming how we monitor the nation's commercial fisheries in the 21st century. Oceanography, 27: 168–174.

Guihen, D., Fielding, S., Murphy, E. J., Heywood, K. J., and Griffiths, G. 2014. An assessment of the use of ocean gliders to undertake acoustic measurements of zooplankton: the distribution and density of Antarctic krill (*Euphausia superba*) in the Weddell Sea. Limnology and Oceanography: Methods, 12: 373–389.

Honkalehto, T., and McCarthy, A. 2015. Results of the Acoustic–Trawl Survey of Walleye Pollock (*Gadus chalcogrammus*) on the U.S. and Russian Bering Sea Shelf in June–August 2014 (DY1407). AFSC Processed Rep. 2015-07. 62 pp. Alaska Fish. Sci. Cent., NOAA, Natl. Mar. Fish. Serv., 7600 Sand Point Way NE, Seattle, WA 98115.

Honkalehto, T., Ressler, P. H., Towler, R., and Wilson, C. D. 2011. Using acoustic data from fishing vessels to estimate walleye pollock abundance in the eastern Bering Sea. Canadian Journal of Fisheries and Aquatic Sciences, 68: 1231–1242.

Karp, W. A. 2007. Collection of acoustic data from fishing vessels. ICES Cooperative Research Reports, 287: 84.

Kieser, R., Mulligan, T. J., Williamson, N. J., and Nelson, M. O. 1987. Intercalibration of two echo integration systems based on acoustic backscattering measurements. Canadian Journal of Fisheries and Aquatic Sciences, 44: 562–572.

Korneliussen, R. J. (Ed). 2018. Acoustic target classification. ICES Cooperative Research Reports, 344: 104.

Kotwicki, S., De Robertis, A., Ianelli, J., Punt, A. E., and Horne, J. K. 2013. Combining bottom trawl and acoustic data to model acoustic dead zone correction and bottom trawl efficiency parameters for semipelagic species. Canadian Journal of Fisheries and Aquatic Sciences, 70: 208–219.

Lemon, D., Johnston, P., Buermans, J., Loos, E., Borstad, G., and Brown, L. 2012. Multiple-frequency Moored Sonar for Continuous Observations of Zooplankton and Fish, pp. 1–6. OCEANS-2012, 14–19 October 2012. Hampton Roads, VA, doi: 10.1109/OCEANS.2012.640491.

Lopez, J., Moreno, G., Lennert-Cody, C., Maunder, M., Sancristobal, I., Caballero, A., and Dagorn, L. 2017. Environmental preferences of tuna and non-tuna species associated with drifting fish aggregating devices (DFADs) in the Atlantic Ocean, ascertained through fishers' echo-sounder buoys. Deep-Sea Research Part II, 140: 127–138.

Macaulay, G. J., Scoulding, B., Ona, E., and Fässler, S. 2018. Comparisons of echo-integration performance from two multi-plexed echosounders. ICES Journal of Marine Science, 6: 2276–2285.

MacLennan, D. N., Fernandes, P. G., and Dalen, J. 2002. A consistent approach to definitions and symbols in fisheries acoustics. ICES Journal of Marine Science, 59: 365–369.

Meinig, C., Lawrence-Slavas, N., Jenkins, R., and Tabisola, H. M. 2015. The use of Saildrones to examine spring conditions in the Bering Sea: vehicle specification and mission performance, pp. 1–6. OCEANS 2015—MTS/IEEE Washington, 19–22 October 2015, Washington, DC, doi: 10.23919/OCEANS.2015.7404348.

Meyer-Gutbrod, E. L., Greene, C. H., and McGarry, L. P. 2015. Wave glider technology for fisheries research. Sea Technology, 2015: 15–19.

Mitson, R. B. (Ed). 1995. Underwater noise of research vessels: review and recommendations. ICES Cooperative Research Reports, 209: 61.

Moline, M. A., Benoit-Bird, K. J., Gorman, D. O., and Robbins, I. C. 2015. Integration of scientific echo sounders with an adaptable autonomous vehicle to extend our understanding of animals from the surface to the bathypelagic. The Journal of Atmospheric and Oceanic Technology, 32: 2173–2186.

Mordy, C., Cokelet, E., De Robertis, A., Jenkins, R., Kuhn, C. E., Lawrence-Slavas, N., Berchok, C. *et al.* 2017. Saildrone surveys of oceanography, fish and marine mammals in the Bering Sea. Oceanography, 30: 113–116.

National Research Council. 2009. Science at Sea: Meeting Future Oceanographic Goals with a Robust Academic Research Fleet. The National Academies Press, Washington, DC.

Novarini, J. C., and Bruno, D. R. 1982. Effects of the sub-surface bubble layer on sound propagation. Journal of the Acoustical Society of America, 72: 510–514.

Ona, E. (Ed). 1999. Methodology for target strength measurements. ICES Cooperative Research Reports, 235: 59.

Ona, E., Godø, O. R., Handegard, N. O., Hjellvik, V., Patel, R., and Pedersen, G. 2007. Silent research vessels are not quiet. Journal of the Acoustical Society of America, 121: 145–150.

Ona, E., and Mitson, R. B. 1996. Acoustic sampling and signal processing near the seabed: the deadzone revisited. ICES Journal of Marine Science, 53: 677–690.

Powell, J. R., and Ohman, M. D. 2015. Changes in zooplankton habitat, behavior, and acoustic scattering characteristics across glider-resolved fronts in the Southern California Current System. Progress in Oceanography, 134: 77–92.

Ressler, P. H., De Robertis, A., Warren, J. D., Smith, J. D., and Kotwicki, S. 2012. Developing an acoustic index of euphausiid abundance to understand trophic interactions in the Bering Sea ecosystem. Deep-Sea Research II, 65–70: 184–195.

Rudnick, D., Costa, D., Johnson, K., Lee, C., and Timmermans, M.-L. (Eds). 2018. ALPS II—Autonomous Lagrangian Platforms and Sensors. A Report of the ALPS II Workshop, 21–24 February, La Jolla, CA. 66 pp.

Ryan, T. E., Downie, R. A., Kloser, R. J., and Keith, G. 2015. Reducing bias due to noise and attenuation in open-ocean echo integration data. ICES Journal of Marine Science, 72: 2482–2493.

Rynne, P., and von Ellenrieder, K. 2009. Unmanned autonomous sailing: current status and future role in sustained ocean observations. Marine Technology Society Journal, 43: 21–30.

Shabangu, F. W., Ona, E., and Yemane, D. 2014. Measurements of acoustic attenuation at 38 kHz by wind-induced air bubbles with suggested correction factors for hull-mounted transducers. Fisheries Research, 151: 47–56.

Simmonds, E. J., and MacLennan, D. N. 2005. Fisheries Acoustics, 2nd edn. Blackwell Science Ltd, Oxford, UK. 437 pp.

Stanton, T. K., Chu, D., Jech, J. M., and Irish, J. D. 2010. New broad-band methods for resonance classification and high-resolution imagery of fish with swimbladders using a modified commercial broadband echosounder. ICES Journal of Marine Science, 67: 365–378.

Swart, S., Zietsman, J. J., Coetzee, J. C., Goslett, D. G., Hoek, A., Needham, D., and Monteiro, P. M. S. 2016. Ocean robotics in support of fisheries research and management. African Journal of Marine Science, 38: 525–538.

Trenkel, V. M., Ressler, P. H., Jech, M., Giannoulaki, M., and Taylor, C. 2011. Underwater acoustics for ecosystem-based management: state of the science and proposals for ecosystem indicators. Marine Ecology Progress Series, 442: 285–301.

Trevorrow, M. V. 2005. The use of moored inverted echo sounders for monitoring meso-zooplankton and fish near the ocean surface. Canadian Journal of Fisheries and Aquatic Sciences, 62: 1004–1018.

Verfuss, U. K., Aniceto, A. S., Harris, D. V., Gillespie, D., Fielding, S., Jimenez, G., Johnston, P. *et al.* 2019. A review of unmanned vehicles for the detection and monitoring of marine fauna. Marine Pollution Bulletin, 140: 17–29.

Handling editor: Olav Rune Godø